



# A Flexible Supercapacitor Based on Niobium Carbide MXene and Sodium Anthraquinone-2-Sulfonate Composite Electrode

Guixia Wang <sup>1,\*</sup>, Zhuo Yang <sup>1</sup>, Xinyue Nie <sup>1</sup>, Min Wang <sup>2,\*</sup> and Xianming Liu <sup>1</sup>

<sup>1</sup> Henan Key Laboratory of Function-Oriented Porous Materials, College of Chemistry and Chemical Engineering, Luoyang Normal University, Luoyang 471934, China; niexinyue0609@163.com (X.N.)

<sup>2</sup> School of Pharmaceutical Sciences, Chongqing University, Chongqing 401331, China

\* Correspondence: author: guixia0116@163.com (G.W.); wang\_min@cqu.edu.cn (M.W.)

**Abstract:** MXene-based composites have been widely used in electric energy storage device. As a member of MXene, niobium carbide (Nb<sub>2</sub>C) is a good electrode candidate for energy storage because of its high specific surface area and electronic conductivity. However, a pure Nb<sub>2</sub>C MXene electrode exhibits limited supercapacitive performance due to its easy stacking. Herein, sodium anthraquinone-2-sulfonate (AQS) with high redox reactivity was employed as a tailor to enhance the accessibility of ions and electrolyte and enhance the capacitance performance of Nb<sub>2</sub>C MXene. The resulting Nb<sub>2</sub>C–AQS composite had three-dimensional porous layered structures. The supercapacitors (SCs) based on the Nb<sub>2</sub>C–AQS composite exhibited a considerably higher electrochemical capacitance (36.3 mF cm<sup>-2</sup>) than the pure Nb<sub>2</sub>C electrode (16.8 mF cm<sup>-2</sup>) at a scan rate of 20 mV s<sup>-1</sup>. The SCs also exhibited excellent flexibility as deduced from the almost unchanged capacitance values after being subjected to bending. A capacitance retention of 99.5% after 600 cycles was observed for the resulting SCs, indicating their good cycling stability. This work proposes a surface modification method for Nb<sub>2</sub>C MXene and facilitates the development of high-performance SCs.

**Keywords:** niobium carbide; MXene; sodium anthraquinone-2-sulfonate; supercapacitors; energy storage; composite electrode



**Citation:** Wang, G.; Yang, Z.; Nie, X.; Wang, M.; Liu, X. A Flexible Supercapacitor Based on Niobium Carbide MXene and Sodium Anthraquinone-2-Sulfonate Composite Electrode. *Micromachines* **2023**, *14*, 1515. <https://doi.org/10.3390/mi14081515>

Academic Editors: Hong Li, Azam Irajizad and Amir Hussain Idrisi

Received: 23 June 2023  
Revised: 25 July 2023  
Accepted: 26 July 2023  
Published: 28 July 2023



**Copyright:** © 2023 by the authors. Licensee MDPI, Basel, Switzerland. This article is an open access article distributed under the terms and conditions of the Creative Commons Attribution (CC BY) license (<https://creativecommons.org/licenses/by/4.0/>).

## 1. Introduction

With the increasing demand for electric energy, electric energy storage has attracted increasing attention from researchers [1–3]. There are several electric energy storage sources, including aqueous Zn–ion batteries [4,5], lithium–selenium batteries [6], Li–ion batteries [7,8], Zn–air batteries [9], ammonium-ion batteries [10], and supercapacitors (SCs) [11–13]. Among them, SCs possess useful characteristics such as ultrahigh power density, long lifetime, and environmental sustainability, and thus, they have become promising electrical energy storage materials for portable electronics and other electric devices [14]. SCs can be divided into electrical double-layer capacitors (EDLCs) and pseudocapacitors in accordance with the energy storage mechanism. Compared with EDLCs, pseudocapacitors usually exhibit much higher capacitances and energy densities through Faradaic redox reactions [1,15]. Pseudocapacitive materials include conducting polymers, electrochemically active organic molecules, and transition metal compounds. As the representative electrochemically active organic molecules, quinones and their derivatives exhibit high redox reactivity, high capacitance, and good adjustable electrochemical reversibility, and they have been used as electrode materials of SCs [16–21]. However, the capacitive performance and long-term cycle stability of SCs based on organic quinones or their derivatives are relatively low due to their low electronic conductivity. To enhance the electronic conductivity of quinones and their derivatives, the Shi group [22] and Zhu group [23] proposed a strategy of using reduced graphene oxide (rGO) as a conductive support of sodium anthraquinone-2-sulfonate (AQS). The resulting SCs based on AQS–rGO composites had enhanced capacitive performance and high capacity retention.

MXenes are a new family of multifunctional two-dimensional (2D) materials comprising transition metal carbides, nitrides, and carbonitrides [24,25]. Titanium carbide MXene-based nanocomposites exhibit good structural stability, electrical properties, and electrocatalytic activity, which makes them very suitable for good matrices of SCs. Niobium carbide ( $\text{Nb}_2\text{C}$ ) MXene has a similarly high electronic conductivity to that of titanium carbide, excellent dispersibility in various solvents, and good compatibility with various components. Recently,  $\text{Nb}_2\text{C}$  MXene has been revealed to be a good electrode candidate for energy storage due to its high specific surface area and high conductivity [26–28]. Both single  $\text{Nb}_2\text{C}$  MXene (denoted as  $\text{Nb}_2\text{CT}_x$ ) [29] as well as composites consisting of  $\text{Nb}_2\text{C}$  MXene delaminated with isopropylamine with carbon nanotubes [30] can be used as electrode materials with excellent cycle stability and Li capacities.

Herein, the organic active molecule AQS was used as a tailor to modify 2D  $\text{Nb}_2\text{C}$  MXene and the resulting  $\text{Nb}_2\text{C}$ –AQS composite was employed to construct a novel SC with high capacitance. The  $\text{SO}_3^-$  functional group in AQS can render AQS soluble in aqueous solutions as well as facilitate the combination of AQS and  $\text{Nb}_2\text{C}$  MXene on the molecular level. Then, the electrochemical capacitance and cycle stability of the SC based on the as-prepared  $\text{Nb}_2\text{C}$ –AQS composite were evaluated and also compared with bare  $\text{Nb}_2\text{C}$  MXene.

## 2. Materials and Methods

### 2.1. Materials and Reagents

$\text{Nb}_2\text{AlC}$  powder was purchased from Forsman Scientific (Beijing, China) Co., Ltd. Hydrofluoric acid (HF, 40%) was from Tianjin Deen Chemical Reagents Co., Ltd., Tianjin, China. Tetrapropylammonium hydroxide (TPAOH, 25 wt%) was from J&K Scientific Co., Ltd., Beijing, China. Sodium anthraquinone-2-sulfonate (AQS, 99%) was purchased from Sigma–Aldrich (St. Louis, MO, USA). Sodium sulfate and other chemicals were all reagent grade quality or better and used without further purification. Aqueous solutions were prepared from deionized water (>18 M·cm, Milli-Q purification system).

### 2.2. Methods

#### 2.2.1. Synthesis of $\text{Nb}_2\text{C}$ MXene

Two-dimensional  $\text{Nb}_2\text{C}$  MXene was prepared by a modified chemical exfoliation method [28].  $\text{Nb}_2\text{AlC}$  powder (ca. 5 g) was slowly added to 30 mL of 40% aqueous HF (Note: HF is highly corrosive) and stirred for 20 h at room temperature. After collection by centrifugation (3500 rpm) and washing with water and anhydrous ethanol, the precipitate was dispersed in 30 mL of aqueous tetrapropylammonium hydroxide under stirring for 10 h at room temperature. The raw  $\text{Nb}_2\text{C}$  materials were collected by centrifugation and washed 3× with ethanol and water to remove the residual TPAOH. Then, the precipitate was dispersed in 100 mL of deionized water and sonicated at 200 W for 30 min. The supernatant was collected and dried in a vacuum oven at 80 °C for 6 h. Thus, the resulting  $\text{Nb}_2\text{C}$  MXene was obtained.

#### 2.2.2. Preparation of $\text{Nb}_2\text{C}$ –AQS Composite

The  $\text{Nb}_2\text{C}$ –AQS composite was prepared by a simple one-step hydrothermal method. Aqueous  $\text{Nb}_2\text{C}$  and AQS (30 mL) with a mass ratio of 1:3 was stirred for 6 h at room temperature. Then, the mixture was transferred into a 50-mL Teflon-lined stainless-steel autoclave and heated at 180 °C for 12 h.  $\text{Nb}_2\text{C}$ –AQS composite was obtained after washing the aforementioned  $\text{Nb}_2\text{C}$ –AQS solution with deionized water 2× and freeze-drying under vacuum.

#### 2.2.3. Characterization

Scanning electron microscopy (SEM) images were acquired on a field-emission Sigma 500 microscope (Carl Zeiss, Jena, Germany). X-ray diffraction (XRD) was measured with a D8 Advance (Bruker, Mannheim, Germany) system. Fourier-transform infrared spec-

tra (FTIR) were obtained with a Nicolet 6700 spectrometer (Thermo Nicolet, Madison, WI, USA).

The electrochemical performance of as-prepared Nb<sub>2</sub>C–AQS was carried out with a three-electrode system in 0.1 mol L<sup>−1</sup> Na<sub>2</sub>SO<sub>4</sub>, with platinum foil as the counter electrode and Ag/AgCl as the reference electrode. The working electrode was fabricated as follows: the as-prepared active material (40 mg), acetylene black, and polytetrafluoroethylene were first mixed in a mass ratio of 75:15:10 in a small quantity of absolute ethanol in a manner that formed a homogeneous slurry. Then, the slurry was coated on a piece of nickel foam (1.0 cm × 1.0 cm), which was dried in a vacuum oven at 80 °C for 12 h and pressed before measurement. Cyclic voltammetry (CV) curves and galvanostatic charge/discharge (GCD) were all performed with a CHI 660E electrochemical workstation (CH Instruments).

### 3. Results and Discussion

#### 3.1. Synthesis and Characterization of Nb<sub>2</sub>C–AQS Composite

Figure 1 illustrate the synthesis process of the Nb<sub>2</sub>C–AQS composite. The morphology of Nb<sub>2</sub>C and the corresponding Nb<sub>2</sub>C–AQS composite was characterized by SEM. Nb<sub>2</sub>C has an accordion-like lamellar structure similar to that of Ti<sub>3</sub>C<sub>2</sub> MXene [24,31], and its layered structure has a large lateral size with almost no defects (Figure 2a). Compared with Nb<sub>2</sub>C, the Nb<sub>2</sub>C–AQS composite maintained the layered structure of Nb<sub>2</sub>C, but it has 3D porous structures (Figure 2b), attributable to the decorated AQS molecules as spacers that suppress aggregation of Nb<sub>2</sub>C MXene. The porous structures of the Nb<sub>2</sub>C–AQS composite can act as ion buffers that facilitate ion transport between the Nb<sub>2</sub>C layers. The exiting of the S element also indicates the successfully assembly of AQS molecules on Nb<sub>2</sub>C MXene surface (Figure 2d–h).

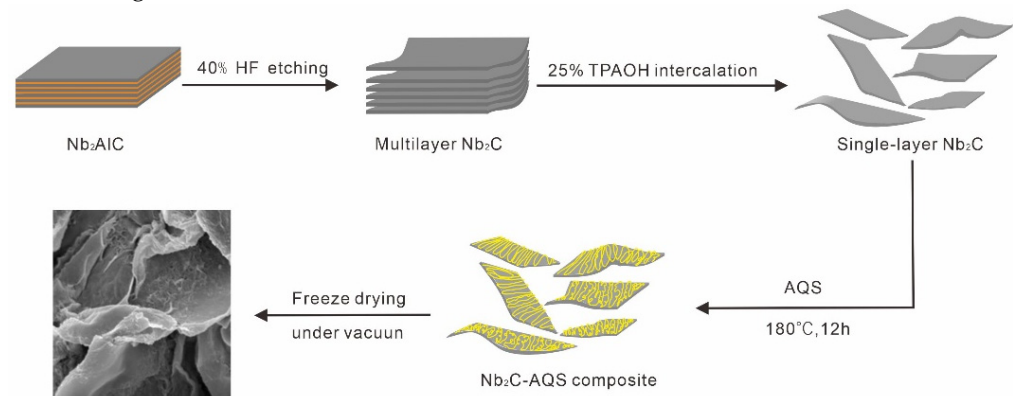


**Figure 1.** Schematic diagram for the fabrication of Nb<sub>2</sub>C–AQS composite.

#### 3.2. Chemical Structure

The XRD patterns indicate formation of Nb<sub>2</sub>C materials (Figure S1, Supporting Information). Only one intense peak of Nb<sub>2</sub>C at ca. 25° was observed, and most of the non-basal plane peaks of Nb<sub>2</sub>AlC bulk (red line in Figure S1, Supporting Information), including the most intense diffraction peak at ca. 39°, were essentially no longer evident after HF treatment and TPAOH intercalation (black line in Figure S1, Supporting Information). Compared with the diffraction patterns of AQS (blue line in Figure 3a), the Nb<sub>2</sub>C–AQS composite had similar XRD patterns, but the peak intensities all decreased, due to interaction of Nb<sub>2</sub>C MXene and AQS molecules (black line in Figure 3a). The FTIR spectra of the Nb<sub>2</sub>C–AQS composite exhibited characteristic peaks of AQS at 1215 and 1660 cm<sup>−1</sup> (Figure 3b), attributable to the asymmetric stretching vibration of –SO<sub>3</sub><sup>−</sup> and the stretching vibration of –C=O from AQS, respectively [32,33]. The zeta potential of the Nb<sub>2</sub>C–AQS composite was −31.8 mV, a much more negative value than that of the Nb<sub>2</sub>C films (−0.19 mV). The results strongly demonstrate the anchoring of AQS onto Nb<sub>2</sub>C MXene.

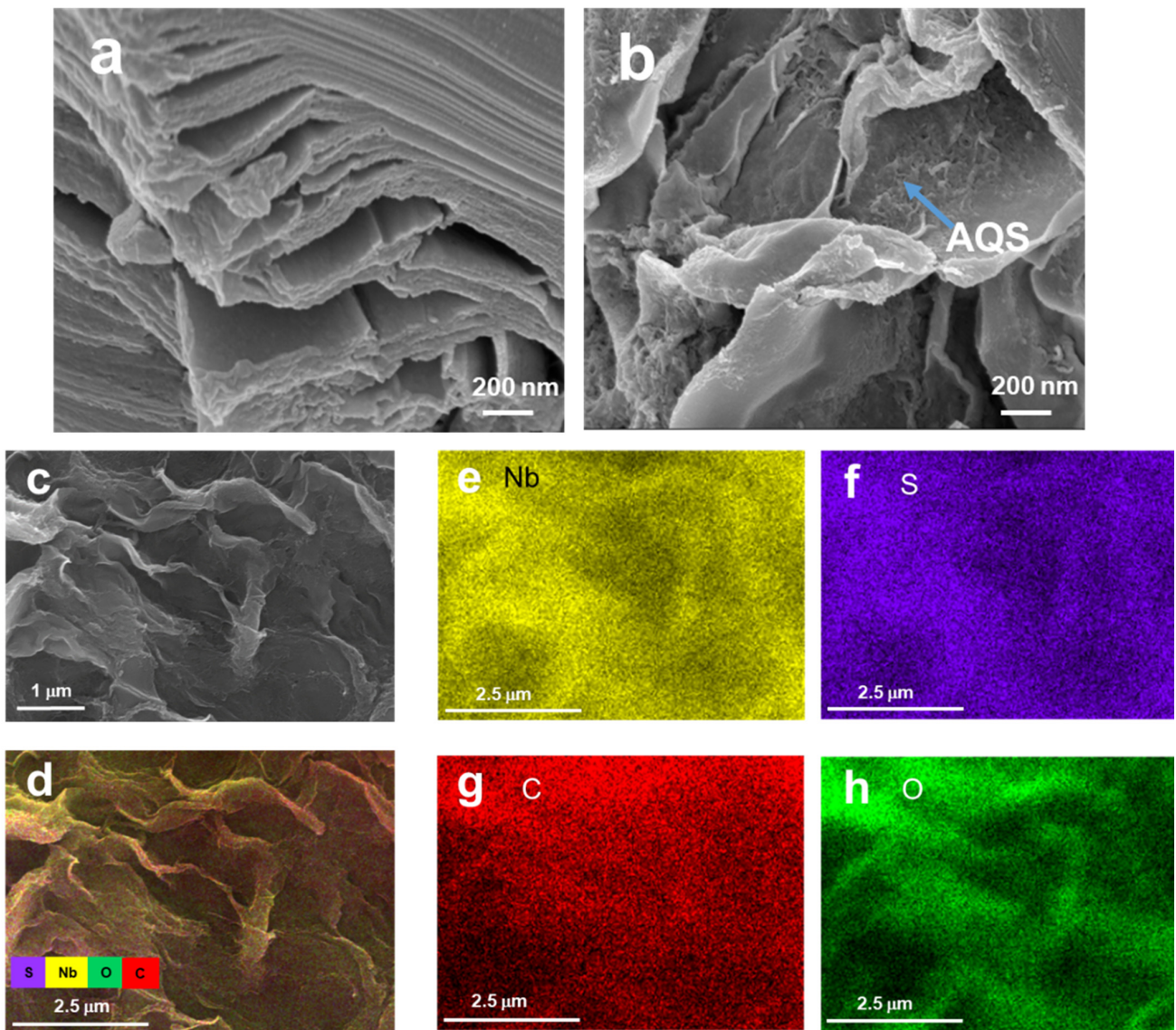


**Figure 2.** SEM images: (a) Nb<sub>2</sub>C layers; (b) and (c): Nb<sub>2</sub>C–AQS composite; (d–h) element mapping of (c).

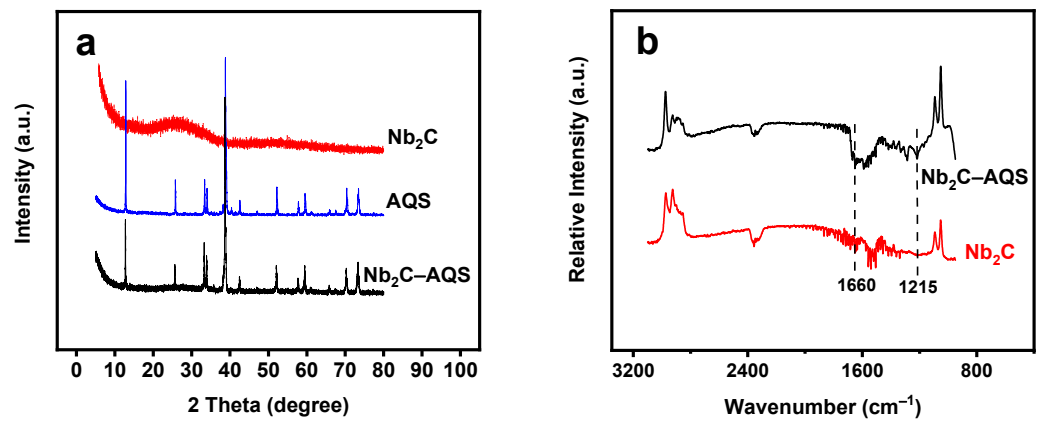


**Figure 3.** (a) XRD patterns of Nb<sub>2</sub>C–AQS, AQS, and Nb<sub>2</sub>C MXene. (b) FTIR spectra of Nb<sub>2</sub>C–AQS and Nb<sub>2</sub>C MXene.

### 3.3. Electrochemical Performance

The obtained Nb<sub>2</sub>C–AQS composite had good conductivity with an equivalent-series resistance (ESR) value of ca. 0.5 Ω derived from its Nyquist plots (Figure S2, Supporting Information). The CV profiles of the Nb<sub>2</sub>C electrode exhibited a nearly rectangular shape at low scan rates in the range of 10–100 mV s<sup>−1</sup> (Figure 4a), which is characteristic of EDLC behavior. Compared with bare Nb<sub>2</sub>C, the resultant device based on the Nb<sub>2</sub>C–AQS composite (denoted as-prepared) exhibited both Faradaic and EDLC capacitance with a pronounced single pair of peaks at ca. 0.22/0.45 V versus Ag/AgCl (at 20 mV s<sup>−1</sup>), originating from the redox reactions of the AQS molecules [22] (Figure 4b). Moreover, the CV curves of Nb<sub>2</sub>C–AQS remained well-defined and symmetric even at a high scan rate of 100 mV s<sup>−1</sup>, suggesting excellent reversibility and stability of the Nb<sub>2</sub>C–AQS electrode. Notably, the peak potentials of the redox peaks slightly shifted with increasing scan rate, which might be due to partial proton-coupled charge transfer between AQS and Nb<sub>2</sub>C. Circa 70% of the capacitance was retained when the scan rate was increased to 100 mV s<sup>−1</sup> (25.4 mF cm<sup>−2</sup>; refer to the Supporting Information for the calculation methods of the specific capacitance), indicating its good rate capability. The Nb<sub>2</sub>C–AQS composite electrode exhibited a considerably higher electrochemical capacitance (36.3 mF cm<sup>−2</sup> at 20 mV s<sup>−1</sup>) than the bare Nb<sub>2</sub>C electrode (16.8 mF cm<sup>−2</sup> at 20 mV s<sup>−1</sup>) (Figure 4c, Table 1); this is mainly due to the high pseudocapacitance of AQS as well as the enhanced accessibility of ions and electrolyte, facilitated by the unique porous structure of the Nb<sub>2</sub>C–AQS composite. The 42.7 mF cm<sup>−2</sup> of specific capacitance for the resulting Nb<sub>2</sub>C–AQS capacitor is higher than that of graphene-based micro-supercapacitors (micro-SCs) (Table 2). The as-prepared SCs display similar capacitance performance as those in some other published works [34–41].

**Table 1.** Electrochemical parameters for as-prepared MSCs in different conditions.

Electrode Materials	Parameters	Areal Capacitance (mF cm <sup>−2</sup> )	Scan Rate
	Nb <sub>2</sub> C–AQS	36.3	20 mV s <sup>−1</sup>
	Nb <sub>2</sub> C	16.8	20 mV s <sup>−1</sup>
	Nb <sub>2</sub> C–AQS	42.7	10 mV s <sup>−1</sup>
	Concavely bent	48.1	10 mV s <sup>−1</sup>
	Convexly bent	40.0	10 mV s <sup>−1</sup>

**Table 2.** Supercapacitance comparison of several composite electrode materials.

Electrode Materials	Specific Capacitance	Test Condition	Ref.
Nb <sub>2</sub> C–AQS	36.3 mF cm <sup>−2</sup>	20 mV s <sup>−1</sup>	This work
PET-CGO-LGO	0.756 mF cm <sup>−2</sup>	20 mV s <sup>−1</sup>	[42]
MPG	0.0807 mF cm <sup>−2</sup>	-	[43]
Ultrathin rGO	0.462 mF cm <sup>−2</sup>	0.1 μA g <sup>−1</sup>	[44]

The CVs of the SCs exhibited similar shapes to that of as-prepared SCs when subjected to bending at a scan rate of 10 mV s<sup>−1</sup> (Figure 4d). The specific capacitances were 48.1 and 40.0 mF cm<sup>−2</sup> for concavely bent and convexly bent SCs (Table 1, bending modes in Figure S3, Supporting Information), respectively, which are almost the same as that of as-prepared SCs (42.7 mF cm<sup>−2</sup>). Thus, the as-prepared SCs have excellent flexibility.

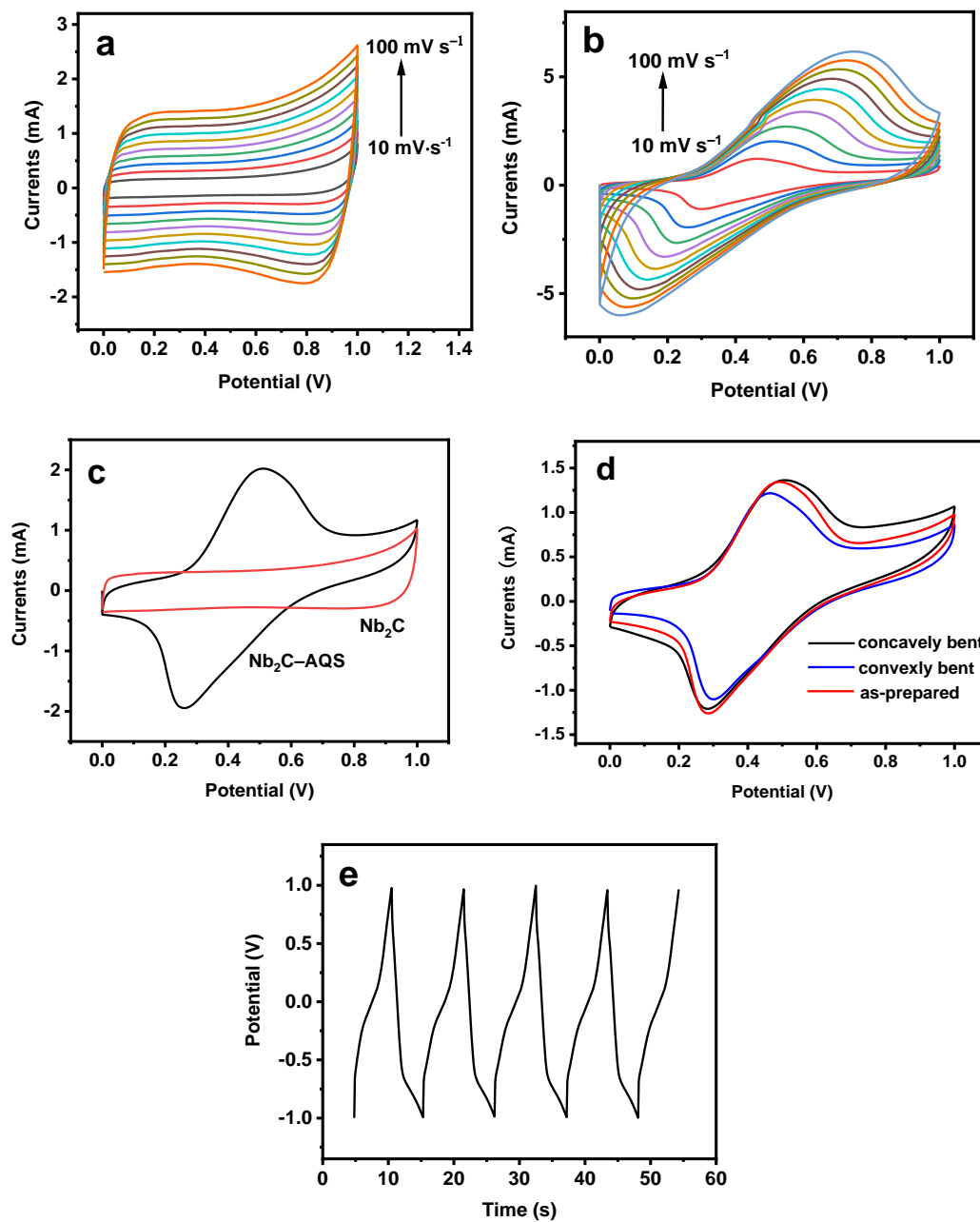


**Figure 4.** CV and GCD curves: (a) CV curves of Nb<sub>2</sub>C MXene and (b) Nb<sub>2</sub>C–AQS composite-based SCs at various scan rates. (c) CV curves of Nb<sub>2</sub>C MXene (red line) and Nb<sub>2</sub>C–AQS composite (black line) at a scan rate of 20 mV s<sup>−1</sup>. (d) CV curves of Nb<sub>2</sub>C–AQS-based SCs (as-prepared, red line), concavely bent (black line), and convexly bent (blue line) at a scan rate of 10 mV s<sup>−1</sup>. (e) GCD curves of the as-prepared SCs at a current density of 15 mA cm<sup>−2</sup>. All the electrochemical measurements were performed in 0.1 mol L<sup>−1</sup> Na<sub>2</sub>SO<sub>4</sub>.

The GCD curves of the Nb<sub>2</sub>C–AQS composite included two parts (Figure 4e): a pair of charge–discharge plateaus attributable to the anchored AQS, and an oblique line stage due to the EDLC behavior of Nb<sub>2</sub>C, which coincides well with the CV curves in Figure 3b. The specific capacitance of the resulting SCs was 36.0 mF cm<sup>−2</sup> at a current density of 15 mA cm<sup>−2</sup> (for the calculation of the specific capacitance, refer to the Supporting Information). In addition, the device exhibited a capacitance retention of 99.5% of its initial capacitance after 600 cycles (Figure S4, Supporting Information), indicating good cycling stability.

#### 4. Conclusions

In summary, AQS was anchored successfully onto the surface of Nb<sub>2</sub>C MXene, and the obtained composite had good conductivity as well as a porous structure. SCs based on the Nb<sub>2</sub>C–AQS composite exhibited a high specific capacitance and good cycling stability. The SCs maintained their initial capacitance when subjected to bending, indicating good flexibility. Compared with bare Nb<sub>2</sub>C MXene, the Nb<sub>2</sub>C–AQS composite electrode provides higher capacitance, which was mainly ascribed to Faradaic redox reactions of the anchored AQS molecules as well as the enhanced accessibility of ions and electrolyte. This work proposes a surface functionalization method for Nb<sub>2</sub>C MXene and also provides a strategy for enhancing the capacitance performance of pure MXene, which will facilitate the development of high-performance SCs.

#### 5. Patents

The results of the patent (a preparation method of a supercapacitor based on 2D niobium carbide nanocomposites, No. ZL2019109099814, China) are from the work reported in this manuscript.

**Supplementary Materials:** The following supporting information can be downloaded at: <https://www.mdpi.com/article/10.3390/mi14081515/s1>, Figure S1: XRD patterns of Nb<sub>2</sub>C nanosheets and Nb<sub>2</sub>AlC powder; Figure S2: Nyquist plots of the Nb<sub>2</sub>C–AQS nanocomposite-modified electrode in 10 mmol L<sup>−1</sup> K<sub>4</sub>Fe(CN)<sub>6</sub> and K<sub>4</sub>Fe(CN)<sub>6</sub> (molar ratio 1:1) from 1–10 mHz at 10 mV sinusoidal signal; Figure S3: Two bending modes of the Nb<sub>2</sub>C–AQS based SC: (a) concavely bent, and (b) convexly bent; Figure S4: Capacitance retention at a current density of 15 mA cm<sup>−2</sup> for the Nb<sub>2</sub>C–AQS-based micro-SC in 0.1 mol L<sup>−1</sup> Na<sub>2</sub>SO<sub>4</sub>.

**Author Contributions:** Conceptualization: G.W. and X.L.; methodology, G.W. and M.W.; investigation, Z.Y.; data curation, G.W. and X.N.; writing—original draft preparation, G.W.; writing—review and editing, X.L. and M.W.; supervision and funding acquisition, G.W. All authors have read and agreed to the published version of the manuscript.

**Funding:** This work was financially supported by the National Natural Science Foundation of China (21305060) and the Training Project for Youth Backbone Teachers in Colleges and Universities of Henan Province (2018GGJS127).

**Data Availability Statement:** All data that support the findings of this study are available within the article and its Supplementary Materials.

**Conflicts of Interest:** The authors declare no conflict of interest.

#### References

1. Wu, Z.; Li, L.; Yan, J.M.; Zhang, X.B. Materials Design and System Construction for Conventional and New-Concept Supercapacitors. *Adv. Sci.* **2017**, *4*, 1600382. [[CrossRef](#)] [[PubMed](#)]
2. Li, L.; Hu, C.; Liu, W.; Shen, G. Progress and Perspectives in Designing Flexible Microsupercapacitors. *Micromachines* **2021**, *12*, 1305. [[CrossRef](#)]
3. Sung, J.; Shin, C. Recent Studies on Supercapacitors with Next-Generation Structures. *Micromachines* **2020**, *11*, 1125. [[CrossRef](#)]
4. Lobinsky, A.A.; Kaneva, M.V.; Tenevich, M.I.; Popkov, V.I. Direct Synthesis of Mn<sub>3</sub>[Fe(CN)<sub>6</sub>]<sub>2</sub>·nH<sub>2</sub>O Nanosheets as Novel 2D Analog of Prussian Blue and Material for High-Performance Metal-Ion Batteries. *Micromachines* **2023**, *14*, 1083. [[CrossRef](#)] [[PubMed](#)]
5. Deng, W.N.; Xu, Y.X.; Zhang, X.C.; Li, C.Y.; Liu, Y.X.; Xiang, K.X.; Chen, H. (NH<sub>4</sub>)<sub>2</sub>Co<sub>2</sub>V<sub>10</sub>O<sub>28</sub>·16H<sub>2</sub>O/(NH<sub>4</sub>)<sub>2</sub>V<sub>10</sub>O<sub>25</sub>·8H<sub>2</sub>O heterostructure as cathode for high-performance aqueous Zn-ion batteries. *J. Alloys Compd.* **2022**, *903*, 163824. [[CrossRef](#)]
6. Deng, W.N.; Li, Y.H.; Xu, D.F.; Zhou, W.; Xiang, K.X.; Chen, H. Three-dimensional hierarchically porous nitrogen-doped carbon from water hyacinth as selenium host for high-performance lithium–selenium batteries. *Rare Met.* **2022**, *41*, 3432–3445. [[CrossRef](#)]
7. Li, D.J.; Guo, H.T.; Jiang, S.H.; Zeng, G.L.; Zhou, W.; Li, Z. Microstructures and electrochemical performances of TiO<sub>2</sub>-coated Mg–Zr co-doped NCM as a cathode material for lithium-ion batteries with high power and long circular life. *New J. Chem.* **2021**, *45*, 19446–19455. [[CrossRef](#)]
8. Ren, L.; Wang, L.; Qin, Y.; Li, Q. High Cycle Stability of Hybridized Co(OH)<sub>2</sub> Nanomaterial Structures Synthesized by the Water Bath Method as Anodes for Lithium-Ion Batteries. *Micromachines* **2022**, *13*, 149. [[CrossRef](#)] [[PubMed](#)]
9. Zhou, W.; Zeng, G.L.; Jin, H.T.; Jiang, S.H.; Huang, M.J.; Zhang, C.M.; Chen, H. Bio-Template Synthesis of V<sub>2</sub>O<sub>3</sub>@Carbonized Dictyophora Composites for Advanced Aqueous Zinc-Ion Batteries. *Molecules* **2023**, *28*, 2147. [[CrossRef](#)] [[PubMed](#)]

10. Wen, X.Y.; Luo, J.H.; Xiang, K.X.; Zhou, W.; Zhang, C.F. Han Chen High-performance monoclinic WO<sub>3</sub> nanospheres with the novel NH<sub>4</sub><sup>+</sup> diffusion behaviors for aqueous ammonium-ion batteries. *Chem. Eng. J.* **2023**, *458*, 141381. [[CrossRef](#)]
11. Xiao, J.L.; Li, H.L.; Zhang, H.; He, S.J.; Zhang, Q.; Liu, K.M.; Jiang, S.H.; Duan, G.G.; Zhang, K. Nanocellulose and its derived composite electrodes toward supercapacitors: Fabrication, properties, and challenges. *J. Bioresour. Bioprod.* **2022**, *7*, 245–269. [[CrossRef](#)]
12. Yang, C.; Li, P.; Wei, Y.; Wang, Y.; Jiang, B.; Wu, W. Preparation of nitrogen and phosphorus doped porous carbon from watermelon peel as supercapacitor electrode material. *Micromachines* **2023**, *14*, 1003. [[CrossRef](#)] [[PubMed](#)]
13. Qian, Y.; Lyu, Z.; Zhang, Q.; Lee, T.H.; Kang, T.K.; Sohn, M.; Shen, L.; Kim, D.H.; Kang, D.J. High-Performance Flexible Energy Storage Devices Based on Graphene Decorated with Flower-Shaped MoS<sub>2</sub> Heterostructures. *Micromachines* **2023**, *14*, 297. [[CrossRef](#)] [[PubMed](#)]
14. Xue, Q.; Gan, H.; Huang, Y.; Zhu, M.; Pei, Z.; Li, H.; Deng, S.; Liu, F.; Zhi, C. Boron element nanowires electrode for supercapacitors. *Adv. Energy Mater.* **2018**, *8*, 1703117. [[CrossRef](#)]
15. Han, Y.; Ge, Y.; Chao, Y.; Wang, C.; Wallace, G.G. Recent progress in 2D materials for flexible supercapacitors. *J. Energy Chem.* **2018**, *27*, 57–72. [[CrossRef](#)]
16. Xie, J.; Shi, H.Z.; Shen, C.; Huan, L.; He, M.X.; Chen, M. Heteroatom-bridged pillar[4]quinone: Evolutionary active cathode material for lithium-ion battery using density functional theory. *J. Chem. Sci.* **2021**, *133*, 1–11. [[CrossRef](#)]
17. Wu, Q.; Sun, Y.; Bai, H.; Shi, G. High-performance supercapacitor electrodes based on graphene hydrogels modified with 2-aminoanthraquinone moieties. *Phys. Chem. Chem. Phys.* **2011**, *13*, 11193–11198. [[CrossRef](#)] [[PubMed](#)]
18. Chen, X.; Wang, H.W.; Yi, H.; Wang, X.F.; Yan, X.R.; Guo, Z.H. Anthraquinone on porous carbon nanotubes with improved supercapacitor performance. *J. Phys. Chem. C* **2014**, *118*, 8262–8270. [[CrossRef](#)]
19. Brousse, K.; Martin, C.; Brisse, A.L.; Lethien, C.; Simon, P.; Taberna, P.L.; Brousse, T. Anthraquinone modification of microporous carbide derived carbon films for on-chip micro-supercapacitors applications. *Electrochim. Acta* **2017**, *246*, 391–398. [[CrossRef](#)]
20. Xu, L.; Shi, R.; Li, H.; Han, C.; Wu, M.; Wong, C.P.; Kang, F.; Li, B. Pseudocapacitive anthraquinone modified with reduced graphene oxide for flexible symmetric all-solid-state supercapacitors. *Carbon* **2017**, *127*, 459–468. [[CrossRef](#)]
21. Boota, M.; Chen, C.; Bécuwe, M.; Miao, L.; Gogotsi, Y. Pseudocapacitance and excellent cyclability of 2,5-dimethoxy-1,4-benzoquinone on graphene. *Energy Environ. Sci.* **2016**, *9*, 2586–2594. [[CrossRef](#)]
22. Shi, R.Y.; Han, C.P.; Duan, H.; Xu, L.; Zhou, D.; Li, H.F.; Li, J.Q.; Kang, F.Y.; Li, B.H.; Wang, G.X. Redox-active organic sodium anthraquinone-2-sulfonate (AQS) anchored on reduced graphene oxide for high-performance supercapacitors. *Adv. Energy Mater.* **2018**, *8*, 1802088. [[CrossRef](#)]
23. Zhu, C.Y.; Zhang, W.J.; Li, G.; Li, C.L.; Qin, X.H. Ultra-simple and green two-step synthesis of sodium anthraquinone-2-sulfonate composite graphene (AQS/rGO) hydrogels for supercapacitor electrode materials. *J. Alloys Compd.* **2021**, *862*, 158472. [[CrossRef](#)]
24. Naguib, M.; Kurtoglu, M.; Presser, V.; Lu, J.; Niu, J.; Heon, M.; Hultman, L.; Gogotsi, Y.; Barsoum, M.W. Two-dimensional nanocrystals produced by exfoliation of Ti<sub>3</sub>AlC<sub>2</sub>. *Adv. Mater.* **2011**, *23*, 4248–4253. [[CrossRef](#)]
25. Kosnan, M.A.; Azam, M.A.; Safie, N.E.; Munawar, R.F.; Takasaki, A. Recent Progress of Electrode Architecture for MXene/MoS<sub>2</sub> Supercapacitor: Preparation Methods and Characterizations. *Micromachines* **2022**, *13*, 1837. [[CrossRef](#)] [[PubMed](#)]
26. Hu, J.P.; Xu, B.; Ouyang, C.Y.; Zhang, Y.; Yang, S.Y. Investigations on Nb<sub>2</sub>C monolayer as promising anode material for Li or non-Li ion batteries from first-principles calculations. *RSC Adv.* **2016**, *6*, 27467–27474. [[CrossRef](#)]
27. Xin, Y.; Yu, Y.X. Possibility of bare and functionalized niobium carbide MXenes for electrode materials of supercapacitors and field emitters. *Mater. Des.* **2017**, *130*, 512–520. [[CrossRef](#)]
28. Lin, H.; Gao, S.; Dai, C.; Chen, Y.; Shi, J.L. A two-dimensional biodegradable niobium carbide (MXene) for photothermal tumor eradication in NIR-I and NIR-II biowindows. *J. Am. Chem. Soc.* **2017**, *139*, 16235–16247. [[CrossRef](#)]
29. Naguib, M.; Halim, J.; Lu, J.; Cook, K.M.; Hultman, L.; Gogotsi, Y.; Barsoum, M.W. New two-dimensional niobium and vanadium carbides as promising materials for Li-ion batteries. *J. Am. Chem. Soc.* **2013**, *135*, 15966–15969. [[CrossRef](#)] [[PubMed](#)]
30. Mashtalir, O.; Lukatskaya, M.R.; Zhao, M.Q.; Barsoum, M.W.; Gogotsi, Y. Amine-assisted delamination of Nb<sub>2</sub>C MXene for Li-ion energy storage devices. *Adv. Mater.* **2015**, *27*, 3501–3506. [[CrossRef](#)] [[PubMed](#)]
31. Wang, G.X.; Yang, Z.; Wu, L.N.; Wang, J.M.; Liu, X.M. Studies on improved stability and electrochemical activity of titanium carbide MXene-polymer nanocomposites. *J. Electroanal. Chem.* **2021**, *900*, 115708. [[CrossRef](#)]
32. Han, Y.Q.; Wang, T.Q.; Li, T.X.; Gao, X.X.; Li, W.; Zhang, Z.; Wang, Y.; Zhang, X.Q. Preparation and electrochemical performances of graphene/polypyrrole nanocomposite with anthraquinone-graphene oxide as active oxidant. *Carbon* **2017**, *119*, 111–118. [[CrossRef](#)]
33. Xu, C.; Cao, Y.; Kumar, R.; Wu, X.; Wang, X.; Scott, K. A polybenzimidazole/sulfonated graphite oxide composite membrane for high temperature polymer electrolyte membrane fuel cells. *J. Mater. Chem.* **2011**, *21*, 11359–11364. [[CrossRef](#)]
34. Duan, G.G.; Xiao, J.L.; Chen, L.; Zhang, C.M.; Jian, S.J.; He, S.J.; Wang, F. Zinc gluconate derived porous carbon electrode assisted high rate and long cycle performance supercapacitor. *J. Energy Storage* **2023**, *67*, 107559. [[CrossRef](#)]
35. Cao, L.H.; Li, H.L.; Liu, X.L.; Liu, S.W.; Zhang, L.; Xu, W.H.; Yang, H.Q.; Hou, H.Q.; He, S.J.; Zhao, Y. Nitrogen, sulfur co-doped hierarchical carbon encapsulated in graphene with “sphere-in-layer” interconnection for high-performance supercapacitor. *J. Colloid Interface Sci.* **2021**, *599*, 443–452. [[CrossRef](#)] [[PubMed](#)]

36. Li, H.L.; Cao, L.H.; Zhang, H.J.; Tian, Z.W.; Zhang, Q.; Yang, F.; Yang, H.Q.; He, S.J.; Jiang, S.H. Intertwined carbon networks derived from Polyimide/Cellulose composite as porous electrode for symmetrical supercapacitor. *J. Colloid Interface. Sci.* **2022**, *609*, 179–187. [[CrossRef](#)] [[PubMed](#)]
37. Guo, W.C.; Guo, X.T.; Yang, L.; Wang, T.Y.; Zhang, M.H.; Duan, G.G.; Liu, X.H.; Li, Y.W. Synthetic melanin facilitates MnO supercapacitors with high specific capacitance and wide operation potential window. *Polymer* **2021**, *235*, 124276. [[CrossRef](#)]
38. Wang, F.; Chen, L.; Li, H.L.; Duan, G.G.; He, S.J.; Zhang, L.; Zhang, G.Y.; Zhou, Z.P.; Jiang, S.H. N-doped honeycomb-like porous carbon towards high-performance supercapacitor. *Chin. Chem. Lett.* **2020**, *31*, 1986–1990. [[CrossRef](#)]
39. Duan, G.G.; Zhao, L.Y.; Chen, L.; Wang, F.; He, S.J.; Jiang, S.H.; Zhang, Q. ZnCl<sub>2</sub> regulated flax-based porous carbon fibers for supercapacitors with good cycling stability. *New J. Chem.* **2021**, *45*, 22602–22609. [[CrossRef](#)]
40. Yang, J.J.; Li, H.L.; He, S.J.; Du, H.J.; Liu, K.M.; Zhang, C.M.; Jiang, S.H. Facile Electrodeposition of NiCo<sub>2</sub>O<sub>4</sub> Nanosheets on Porous Carbonized Wood for Wood-Derived Asymmetric Supercapacitors. *Polymers* **2022**, *14*, 2521. [[CrossRef](#)]
41. Duan, G.G.; Zhang, H.; Zhang, C.M.; Jiang, S.H.; Hou, H.Q. High mass-loading  $\alpha$ -Fe<sub>2</sub>O<sub>3</sub> nanoparticles anchored on nitrogen-doped wood carbon for high-energy-density supercapacitor. *Chin. Chem. Lett.* **2023**. [[CrossRef](#)]
42. Wang, G.X.; Babaahmadi, V.; He, N.; Liu, Y.; Pan, Q.; Montazer, M.; Gao, W. Wearable supercapacitors on polyethylene terephthalate fabrics with good wash fastness and high flexibility. *J. Power Sources* **2017**, *367*, 34–41. [[CrossRef](#)]
43. Wu, Z.; Parvez, K.; Feng, X.; Müllen, K. Graphene-based in-plane micro-supercapacitors with high power and energy densities. *Nat. Commun.* **2013**, *4*, 2487. [[CrossRef](#)] [[PubMed](#)]
44. Niu, Z.; Zhang, L.; Liu, L.; Zhu, B.; Dong, H.; Chen, X. All-solid-state flexible ultrathin micro-supercapacitors based on graphene. *Adv. Mater.* **2013**, *25*, 4035–4042. [[CrossRef](#)]

**Disclaimer/Publisher’s Note:** The statements, opinions and data contained in all publications are solely those of the individual author(s) and contributor(s) and not of MDPI and/or the editor(s). MDPI and/or the editor(s) disclaim responsibility for any injury to people or property resulting from any ideas, methods, instructions or products referred to in the content.